International Journal of Thermal Sciences 49 (2010) 909–921

Contents lists available at ScienceDirect

International Journal of Thermal Sciences

journal homepage: www.elsevier.com/locate/ijts

Two-phase flow distribution in multiple parallel tubes

N. Ablanque, C. Oliet, J. Rigola, C.D. Pérez-Segarra, A. Oliva*

Centre Tecnològic de Transferència de Calor (CTTC), Universitat Politècnica de Catalunya (UPC), ETSEIAT, c. Colom 11, 08222 Terrassa (Barcelona), Spain

ARTICLE INFO

Article history:
Received 24 March 2009
Received in revised form
10 September 2009
Accepted 6 November 2009
Available online 6 February 2010

Keywords:
Two-phase flow
Distribution
Modelling
Manifold systems
T-junctions

ABSTRACT

This work is focussed on the development of a numerical simulation model that predicts the thermal and fluid-dynamic behaviour of the two-phase flow distribution in systems with multiple branching tubes like manifolds. The geometry of a simulated branching system is represented as a set of tubes connected together by means of junctions. On one side, the in-tube evaporation/condensation phenomena are simulated by means of a one-dimensional two-phase flow model, and on the other side, the splitting/converging flow phenomena occurring at junctions are predicted with appropriate junction models obtained from the technical literature. The global flow distribution is calculated using a semi-implicit pressure based method (SIMPLE-like algorithm) where the continuity and momentum equations of the whole domain are solved and linked with both the in-tube two-phase flow model and the junction models.

In the present paper, the flow distribution model is described and its most significant aspects are detailed. Furthermore, the model is validated against experimental and numerical data found in the open literature. The numerical predictions are compared against an adiabatic single-phase flow manifold system working with water and also against a two-phase flow upwardly oriented manifold system working with carbon dioxide. In addition to this, a numerical comparison of a manifold system with two different orientations is carried out. Concluding remarks about the possibilities that this kind of model offers are presented in the last section.

1. Introduction

In many heat exchangers, such as those used in refrigerating systems, the inner fluid is distributed in several tubes in order to have high cycle performance and small equipment size (Watanabe et al. [1]). The flow distribution is usually achieved by means of manifold/header systems. A typical arrangement includes a dividing manifold, a set of parallel tubes where the heat transfer process takes place, and a combining manifold where the whole flow is regrouped again. In general, a heat exchanger performs better when the mass flow rate is uniformly distributed through the intermediate tubes. However, an uneven distribution may occur and the heat exchanger thermal and hydraulic performance is deteriorated. This maldistribution situation is particularly unfavourable for two-phase flows due to the possible uneven phase split at each junction of the dividing manifold.

In an evaporator with unequal flow distribution the heat transfer vary from tube to tube depending on both the tube flow conditions (e.g. mass flow rate, inlet gas weight fraction) and the external heat load. This situation may lead to the undesirable presence of the dry-out phenomena – or an earlier set than the expected – in some tubes. Consequently, the heat transferred by these tubes will steeply decrease as well as the global heat exchanger performance. A uniform phase distribution is also recommended for better heat transfer performance in condensers. Thus, the prediction of the flow distribution in a manifold is a crucial aspect for the heat exchanger design optimisation.

During the last decades, a significant amount of experimental and numerical research works have been focussed on studying the flow distribution in manifold/header systems. Different works dealing with single-phase fluids have shown that the flow distribution depends mainly on the pressure drop related to both the friction through tubes and the flow split at junctions [2–4]. However, when two-phase flows are considered the flow distribution prediction becomes a harder task. The phase split phenomena are very complex and depend not only on geometric parameters (size, shape, position and orientation of both the manifold and the tubes), but also on the flow conditions (mass velocity, gas weight fraction, flow pattern) and on the heat load applied to each tube (Mueller and Chiou [5]). Research efforts have been done for a wide variety of fluids, operating conditions, heat exchanger types and geometries. The most relevant experimental

* Corresponding author. Tel.: +34 937398101.
E-mail address: oliva@cttc.upc.edu (A. Oliva).

1290-0729/$ – see front matter © 2009 Elsevier Masson SAS. All rights reserved.
doi:10.1016/j.ijthermalsci.2009.11.005

studies and numerical attempts carried out on this topic are summarised in both Hwang et al. [6] and Marchitto et al. [7]. In fact, no general two-phase flow distribution prediction model has been proposed.

The aim of this work is the development of a numerical model to predict the flow distribution in systems with branching conduits. The basic idea of the model is to represent the studied domain as a set of tubes connected by means of junctions. Both the fluid-dynamic and the heat transfer phenomena occurring inside the tubes and manifolds are solved with a two-phase flow in-tube one-dimensional model [8]. The pressure change in all junctions and the phase split at dividing junctions are solved using appropriate junction models found in the open literature [9–13]. The global resolution procedure consists on solving the mass and momentum equations applied to the whole system and to relate them with both the fluid and the junction models in order to predict the thermal behaviour and the flow distribution of the studied domain. The first numerical results of the flow distribution simulation model were presented in Oliet et al. [14].

In the following section the model is described in detail. In the third section, the model is validated against experimental data and numerical results from other authors. Two main experimental cases are considered: a single-phase flow manifold system working with water, and a two-phase flow manifold system working with carbon dioxide. The former represents a solar collector and the latter consists of an upwardly oriented automotive air conditioner evaporator. In the fourth section, a numerical comparative study for the carbon dioxide evaporators is carried out in order to show the model capabilities. Finally, concluding remarks are presented.

2. Numerical model

The global numerical resolution process is based on the coupling of three different numerical models related to: i) the phase split and the pressure drop occurring at junctions; ii) the thermal and the fluid-dynamic behaviour of the two-phase flow through tubes and manifolds themselves; and iii) the global momentum and continuity conservation governing equations coupled over the whole manifold system. In the following sections both the domain discretization and the main details of the resolution process are described.

2.1. Domain discretization

The discretization has been developed at two different levels. The higher level represents the whole heat exchanger which is discretized by means of nodes (placed at branch ends) and branches (tubes/channels between two adjacent nodes) as shown in Fig. 1(a). The working fluid state is defined at each node by means of two properties, the pressure and the enthalpy, while its mass flow rate is defined at each branch. These values are calculated with the resolution algorithm presented in Section 2.5.

The lower level represents the manifold system branches (e.g. manifold parts between two adjacent junctions and tubes placed between manifolds). The branches are divided in concatenated control volumes that may represent different types of elements, such as: dividing junctions, combining junctions, tubes, etc. The flow pressure and enthalpy evolution between the upstream and downstream positions of an element (or control volume) depends on the element specific characteristics, while the pressure variation through the whole branch is obtained from the integration of its elements along the whole fluid path (see Section 2.5). The diagram depicted in Fig. 1(b) shows the typical branch elements found on a heat exchanger tube situated between the dividing and the combining manifolds. In this case, the behaviour of the first element is characterised from an appropriate dividing T-junction model (see Section 2.2), the second element is modelled by means of a two-phase flow numerical model (see Section 2.3), and the last element is characterised from a convenient converging T-junction model (see Section 2.2).

Each branch is defined from an origin to a destination node which do not necessarily agree with the flow direction. These nodes represent junctions and they are equivalent to the nodes depicted in Fig. 1(a). The fluid state (enthalpy and pressure) and its mass flow rate are defined for the three nodes placed at the junction ends (branch, run and inlet). In fact the working fluid state of the branch origin/destination node corresponds to the T-junction inlet/run node depending on the flow direction.

2.2. T-junction models

Appropriate junction models are needed in order to predict the pressure change (in dividing and combining T-junctions) and the phase split (in two-phase flow dividing junctions) of a whole heat exchanger manifold system. However, the reliable use of these models – specially for the phase split prediction – is limited to their experimental ranges and conditions. It should be also considered that some effects that may occur in a manifold system (e.g. backward flow, influence of adjacent junctions) are not usually taken into account by the models. In this section the specific T-junction models used in this work for both single- and two-phase flows are briefly described. The dividing and combining junctions are defined as shown in Fig. 1(b).

2.2.1. Pressure change evaluation

The expressions reported in Idelchik [13] are used to predict the pressure variation in single-phase dividing and combining T-junctions as they cover a wide variety of operational and geometrical conditions. The pressure variations through a dividing T-junction are calculated as follows:

$$(\Delta p)_{ru-in} = \rho\frac{v_{ru}^2}{2}\left(\xi_{ru} - 1 + \left(\frac{v_{in}}{v_{ru}}\right)^2\right) \tag{1}$$

$$(\Delta p)_{br-in} = \rho\frac{v_{br}^2}{2}\left(\xi_{br} - 1 + \left(\frac{v_{in}}{v_{br}}\right)^2\right) \tag{2}$$

where the flow resistance coefficients (ξ) depend on the Reynolds number, on the T-junction cross-sectional areas (S_{in}, S_{ru} and S_{br}) and on the volumetric flow rates. They include all the sources of pressure loss occurring at junctions (sudden expansions, flow turning, turbulent mixing, friction through passages, etc.) and are calculated with additional expressions and empirical values also reported by Idelchik [13]. Similar expressions are used for single-phase combining T-junctions.

For predicting the pressure change in two-phase flow dividing T-junctions several models have been presented in the literature and a summary is given by Buell et al. [15]. The model implemented in this work is reported in Tae and Cho (12) and considers both the reversible pressure variation (due to the flow rate decrease) and the irreversible pressure variation (due to the change of the flow direction and the orifice losses). The irreversible term is only considered for predicting the pressure variation between the inlet and branch positions:

$$(\Delta p)_{ru-in} = (\Delta p)_{ru-in,rev} \tag{3}$$

$$(\Delta p)_{br-in} = (\Delta p)_{br-in,rev} + (\Delta p)_{br-in,irrev} \tag{4}$$

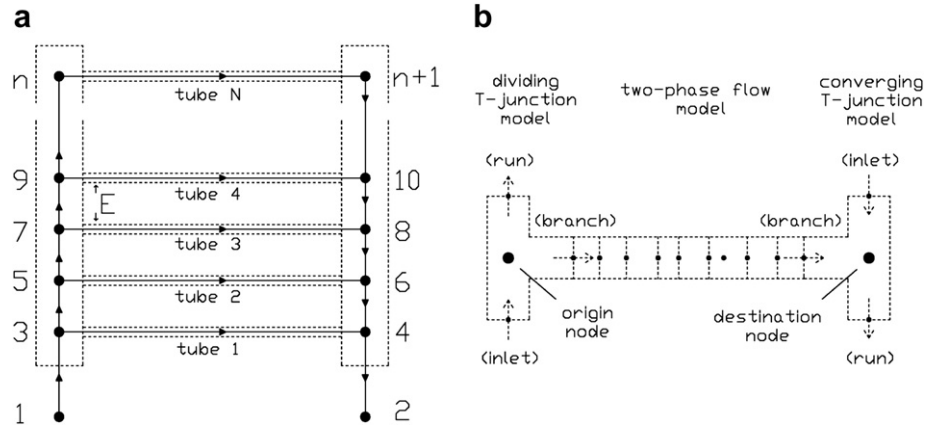

Fig. 1. Domain discretization: (a) heat exchanger grid and (b) typical branch elements; T-junctions characterisation in brackets.

The reversible term is calculated based on the two-phase Bernoulli equation while the irreversible term is calculated from a single-phase pressure loss coefficient and a two-phase local loss multiplier.

Few models are reported in the literature for predicting the pressure change of two-phase flows through combining T-junctions. However, Schmidt and Loth [16] presents three different models derived from existing models for dividing T-junctions. The model used in this work is the so-called "contraction coefficient model" which considers that both incoming flows (branch and inlet) are contracted as they come together. The model main idea is to divide each flow path into two regions: before their maximal contraction and after it.

$$(\Delta p)_{br-ru} = (\Delta p)_{br-ru,before} + (\Delta p)_{br-ru,after} \tag{5}$$

$$(\Delta p)_{in-ru} = (\Delta p)_{in-ru,before} + (\Delta p)_{in-ru,after} \tag{6}$$

The first term is assumed to be non-dissipative while the second term is considered dissipative. They are calculated by means of an energy and a momentum balance respectively. The flow path cross-section at its maximal contraction is estimated from empirical contraction coefficients.

2.2.2. Phase split

The correlation presented by Seeger et al. [9] is used to predict the phase split in T-junctions with an horizontal main tube and a vertical upward oriented branch (H–VU). This correlation is purely empirical and consists on a very simple relation between the inlet flow conditions and the branch flow conditions:

$$\frac{x_{g,br}}{x_{g,in}} = \left(\frac{\dot{m}_{br}}{\dot{m}_{in}}\right)^{-0.8} \tag{7}$$

The correlation was based on experiments where the flow parameters were varied over a wide range in order to consider different inlet flow patterns. The influence of inlet conditions was found to be relatively small. Once the gas weight fraction at the branch position ($x_{g,\,br}$) is known, the gas weight fraction at the run position ($x_{g,\,ru}$) is deduced from the phase conservation equation ($\dot{m}_{in}x_{g,in} = \dot{m}_{br}x_{g,br} + \dot{m}_{ru}x_{g,ru}$).

For T-junctions with both the main tube and the branch placed horizontally (H–H) the phenomenological semi-empirical model of Hwang et al. [10] is used. The model is based on a force balance over dividing streamlines for gas and liquid where the centrifugal and the interfacial drag forces are assumed to be dominant. However, for a separated two-phase flow such as stratified or annular, the interfacial drag force is relatively small and the model simplifies to a balance between centrifugal forces:

$$\frac{\rho_g v_g^2}{R_g} = \frac{\rho_l v_l^2}{R_l} \tag{8}$$

On one side, the radius of curvature of each streamline (R) is calculated from an empirical expression provided by Hwang et al. [10] which is related to the positions of the liquid and gas streamlines. On the other side, the branch liquid fraction intake $\dot{m}_{br}(1-x_{g,br})/\dot{m}_{in}(1-x_{g,in})$ and the branch gas fraction intake $(\dot{m}_{br}x_{g,br}/\dot{m}_{in}x_{g,in})$ are also related to the positions of the liquid and gas streamlines by means of geometrical relations that depend on the inlet flow pattern. In this case, the value of $x_{g,br}$ is obtained iteratively and $x_{g,ru}$ is deduced from the phase conservation equation.

Illustrative results are shown in Fig. 2 where the dividing T-junction model of Hwang et al. [10] is compared against both annular and stratified flow experimental data. The annular flow regime experimental data were taken from Tae and Cho [12] (where specific geometric equations to represent the annular flow regime in the Hwang et al. model were reported) while the stratified flow regime experimental data were obtained from Marti and Shoham [11] (in this case, the corresponding geometric equations have been deduced).

Finally, an important aspect to mention is that the flow pattern of the inlet flow at each dividing T-junction must be predicted in order to select the appropriate T-junction model. In the present flow distribution model the flow pattern map used is that of Thome [17] which is specific for horizontal tubes (in this work the main tube of the dividing manifold is always horizontally oriented).

2.3. Numerical simulation of in-tube two-phase flow and the solid elements

The numerical simulation model of the thermal and fluid-dynamic behaviour of two-phase flow inside tubes is carried out from the integration of the fluid conservation equations along the flow domain, which is split into a number of finite control volumes as is shown in Fig. 3. Considering a steady-state quasi-homogeneous fully-implicit one-dimensional model, the discretized governing equations (continuity, momentum and energy) show the following form:

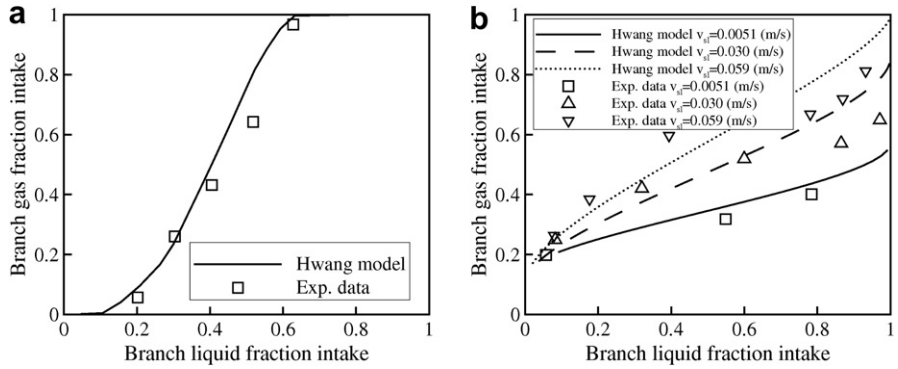

Fig. 2. Hwang et al. [10] model for horizontal T-junctions compared against experimental data from: (a) Tae and Cho [12] -annular regime- and (b) Marti and Shoham [11]-stratified regime.

$$\dot{m}_i - \dot{m}_{i-1} = 0 \tag{9}$$

$$\dot{m}_i v_i - \dot{m}_{i-1} v_{i-1} = (p_{i-1} - p_i)S - \bar{\tau}_i \pi D \Delta z_i - \bar{\rho}_i g \sin(\theta) S \Delta z_i \tag{10}$$

$$\dot{m}_i (h_i + e_{c,i} + e_{p,i}) - \dot{m}_{i-1}(h_{i-1} + e_{c,i-1} + e_{p,i-1}) = \bar{q}_i \pi D \Delta z_i \tag{11}$$

In these equations: i) the mean control volume variables (e.g. velocity, pressure, temperature, etc.) are calculated from an arithmetic mean between their values at the inlet and outlet faces ($\bar{\phi}_i \approx (\phi_i + \phi_{i-1})/2$); ii) the two-phase flow velocity is expressed from the gas and liquid velocities ($v_i = v_{g,i} x_{g,i} + v_{l,i}(1 - x_{g,i})$), which are calculated by means of both the gas weight fraction and the void fraction (e.g. $v_{g,i} = (\dot{m}_i x_{g,i})/(\rho_{g,i} \epsilon_{g,i} S)$); and iii) the two-phase density is estimated from the void fraction value ($\rho_i = \rho_{g,i} \epsilon_{g,i} + \rho_{l,i}(1 - \epsilon_{g,i})$).

The fluid formulation requires the use of empirical correlations (see Section 2.4) to evaluate three specific parameters: the local void fraction ($\epsilon_{g,i}$), the local shear stress which is usually calculated from a friction factor ($\bar{\tau}_i = (f_i/4)(\dot{m}^2/2\bar{\rho}_i S^2)$), and the local heat transfer coefficient (α_i) used to evaluate the heat transferred between the tube and the fluid ($\bar{q}_i = \alpha_i (T_{wall,i} - \bar{T}_i)$).

The resolution is carried out on the basis of a step-by-step numerical scheme. The governing equations are rearranged and solved for the i position. Thus, from the inlet flow conditions at the current instant (i.e. $\dot{m}_1, p_1, h_1$) each control volume outlet state is calculated sequentially. The tube wall temperature map acts as the boundary condition for the whole internal flow.

The energy balance over the solid part of the tube is also considered. The tube is discretized in a way, that for each fluid flow control volume, there is a corresponding tube temperature (see Fig. 3). The balance takes into account the conduction heat transfer along the tube together with the heat exchanged with the internal fluid and the heat transferred to/from the external environment. The energy equation applied at each solid control volume is expressed as follows:

$$-\lambda_{i_-} \frac{T_i - T_{i-1}}{z_i - z_{i-1}} S + \lambda_{i_+} \frac{T_{i+1} - T_i}{z_{i+1} - z_i} S + \bar{q}_{ext,i} \pi D_{ext} \Delta z_i - \bar{q}_i \pi D \Delta z_i = 0 \tag{12}$$

where $\bar{q}_{ext,i}$ is evaluated according to the external conditions (external flow, insulation cover, etc.). The fact of linking the tube temperatures has two important consequences: the numerical resolution procedure becomes more stable, and the tube temperature map becomes more realistic.

The process of solving in a segregated way the inner fluid, the solid tube and the external condition (if necessary), is carried out iteratively until a converged solution is obtained. The solution is given when all the variables (mass flow rate, pressure, enthalpy, tube temperatures and external variables) agree with the convergence criteria in order to obtain the desired accuracy ($|(\phi^* - \phi)/\phi| \leq \xi$). The simulation of the fluid phenomena in transient situations is limited due to the fact that most of the empirical correlations that feed the model are specific for steady state conditions. More details of the model are found in García-Valladares et al. [8].

2.4. Empirical correlations

In this section a brief description of the empirical correlations (friction factor, heat transfer coefficient and void fraction) used in the two-phase flow model is given.

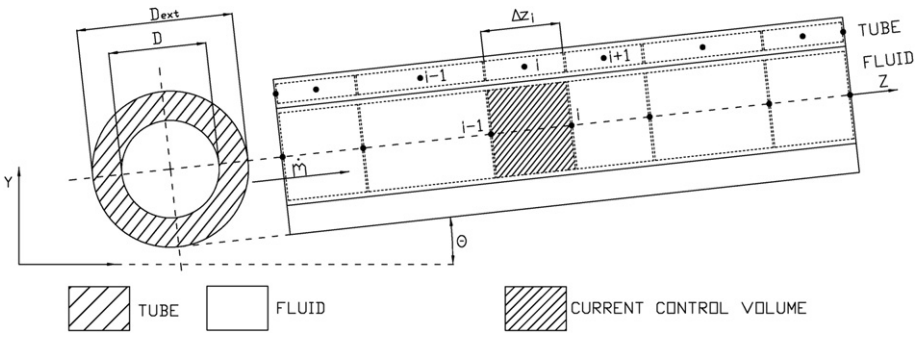

Fig. 3. Fluid flow and tube one-dimensional discretization.

2.4.1. Friction factor/shear stress

When the flow is at single-phase condition, the friction factor is calculated from the often quoted correlation of Churchill [18]. This correlation was written to curve fit the Moody diagram without involving any iterative process. The friction factor is obtained explicitly from the flow Reynolds number and the tube roughness:

$$f = 8\left[\left(\frac{8}{\mathrm{Re}}\right)^{12} + \frac{1}{(A+B)^{3/2}}\right]^{1/12} \tag{13}$$

$$A = \left[2.457\ln\left[\left(\frac{7}{\mathrm{Re}}\right)^{0.9} + 0.27\frac{\varepsilon}{D}\right]^{-1}\right]^{16}$$
$$B = \left(\frac{37530}{\mathrm{Re}}\right)^{16} \tag{14}$$

In case of two-phase flow situations, the shear stress is predicted from the liquid single-phase shear stress and a two-phase flow multiplier ($\tau_{tp} = \phi^2\tau_l$). The two-phase flow multiplier is calculated by means of the Friedel correlation [19]:

$$\phi^2 = E + \frac{3.23FH}{Fr^{0.045}We^{0.035}} \tag{15}$$

where the parameters E, F and H are calculated from additional expressions which depend on the fluid properties at the liquid/gas saturation states and on the single-phase friction factor coefficient (estimated with the correlation of Churchill).

2.4.2. Heat transfer coefficient

The heat transfer coefficient for single-phase flows is calculated with the correlation proposed by Gnielinski [20] which was tested in smooth tubes and for a wide range of experimental conditions:

$$\mathrm{Re} \geq 2000 \quad Nu = \frac{(f/8)(\mathrm{Re}-1000)\mathrm{Pr}}{1+12.7\sqrt{(f/8)}\left(\mathrm{Pr}^{2/3}-1\right)}$$
$$\mathrm{Re} < 2000 \quad Nu = 3.66 \tag{16}$$

The heat transfer coefficient for evaporation in two-phase flows is estimated with the correlation of Gungor and Winterton [21] where the convective and nucleate boiling heat transfer coefficients are added ($\alpha_{tp} = E\alpha_{cb} + S\alpha_{nb}$). The nucleate boiling contribution is calculated with the pool boiling equation of Cooper [22] multiplied by a suppression factor (S), and similarly, the convective contribution is obtained from the well-known Dittus–Boelter Equation [23] multiplied by an enhancement factor (E). This correlation was developed from many fluids data. In a subsequent article, Gungor and Winterton [24] suppressed the nucleate boiling contribution term and replaced it by a simpler expression:

$$\alpha_{tp} = E\alpha_l \tag{17}$$

$$E = 1 + 3000Bo^{0.86} + 1.12\left(\frac{x_g}{1-x_g}\right)^{0.75}\left(\frac{\rho_l}{\rho_g}\right)^{0.41} \tag{18}$$

where the liquid heat transfer coefficient (α_l) is evaluated with the Dittus–Boelter equation.

In addition to this, a specific correlation to determine the dry-out position and to predict the heat transfer coefficient in this region was also implemented (Groeneveld [25]).

2.4.3. Void fraction

In two-phase flow conditions the void fraction (ϵ_g) is predicted from a slip ratio correlated equation. The approach consists in assuming that the liquid and vapor phases are separated into two streams that flow through the tube with different velocities, v_g and v_l, the ratio of which is given by the split ratio (v_g/v_l).

$$\epsilon_g = \frac{1}{1+\left(\frac{1-x_g}{x_g}\right)\left(\frac{\rho_g}{\rho_l}\right)\left(\frac{v_g}{v_l}\right)} \tag{19}$$

In this work the split ratio was estimated from the expression reported by Premoli et al. [26].

2.5. Numerical simulation of flow distribution in assembled branches

The global flow distribution through the whole manifold system is calculated by means of a flexible approach that couples the T-junctions models with the in-tube two-phase flow model. The global solution is obtained iteratively by solving three different steps as follows:

- The first step consists on defining the pressure behaviour of branches. As shown in Fig. 1(b), each branch is composed of different elements such as T-junctions and tubes (each element may be split in two or several control volumes). The branch is solved, element by element, from its current mass flow rate and the working fluid conditions at its upstream node. The pressure change through each control volume is expressed by means of the following expression:

$$(p_oS_o - p_dS_d)_i = A_{1,i}|\dot{m}|\dot{m} + A_{2,i}\dot{m}^2 + B_i\dot{m} + C_i \tag{20}$$

  where A_1, A_2, B and C represent coefficients to be determined, and the subindexes o (origin) and d (destination) indicate the branch ends which do not necessarily agree with the flow direction. For a T-junction control volume these coefficients are obtained by rearranging the momentum equation of the corresponding T-junction model (see Section 2.2). For the fluid control volumes, the coefficients are obtained by rearranging the momentum equation of the two-phase flow model (Equation 10). Then the pressure coefficients of all the branch control volumes are sequentially added and the momentum equation of each whole branch is defined as follows:

$$p_oS_o - p_dS_d = \left(\sum A_{1,i}\right)|\dot{m}|\dot{m} + \left(\sum A_{2,i}\right)\dot{m}^2 + \left(\sum B_i\right)\dot{m} + \sum C_i \tag{21}$$

- The second step consists on characterising the thermal behaviour of the whole branch by means of the two-phase flow model (heat transfer in junctions is neglected). In the case of a branch placed between the dividing and the combining manifold, the inlet conditions needed to feed the two-phase flow model are obtained from the branch upstream T-junction outlet conditions. Then, after solving the two-phase flow model (see Section 2.3), the enthalpy variation along the whole branch is known.
- The third step consists on solving the whole flow distribution (mass flow values in branches and pressure values at nodes). To predict the flow distribution, a one-dimensional adaptation of the SIMPLE method has been implemented (Patankar [27]). In this sense, an expression for the mass flow at each branch is deduced from Equation (21):

$$\dot{m} = \frac{p_oS_o - p_dS_d - \sum C_i}{\left(\sum A_{1,i}\right)|\dot{m}| + \left(\sum A_{2,i}\right)\dot{m} + \sum B_i} = d_{od}\left(p_oS_o - p_dS_d - \sum C_i\right) \tag{22}$$

The algorithm starts with a guessed pressure field (p^*). The mass flow predicted by the momentum equation ($\dot{m}^*$) should be modified by a correction mass flow ($\dot{m}'$) in order to determine an updated mass flow ($\dot{m}$) that accomplishes the continuity equation. Based in the linear momentum expression (Equation 22) the correction mass flow is evaluated from the correction pressures (p') as follows:

$$\dot{m}' = d_{od}\left(p'_o S_o - p'_d S_d\right) \tag{23}$$

Considering the relation between flows ($\dot{m} = \dot{m}^* + \dot{m}'$) together with Equation (23), the mass conservation equation applied at each node of the discretized manifold system ($\sum \dot{m} = 0$) takes the following form:

$$\sum_{i=\text{node as } o} d_{od,i}\left(p'_{node} S_{o,i} - p'_{d,i} S_{d,i}\right) - \sum_{i=\text{node as } d} d_{od,i}\left(p'_{o,i} S_{o,i} - p'_{node} S_{d,i}\right) = \sum \dot{m}^* \tag{24}$$

The set of mass conservation equations is solved and new values of p' are obtained. From the predicted and correction values, new values of pressure are determined ($p = p^* + p'$). The convergence is reached iteratively. More information about the resolution procedure is detailed in Oliet [28].

The boundary conditions needed for the resolution can be applied at any node of the manifold system mesh. For a manifold system it will be enough to define the mass flow or the pressure at the inlet/outlet nodes (nodes 1 and 2 of Fig. 1).

2.6. Global numerical algorithm

The steady state solution of a flow distribution through a heat exchanger with parallel tubes is obtained iteratively as follows:

1. The temperature map of all the tubes (solid part) is guessed or defined. Furthermore, both the working fluid state at nodes and the mass flow in branches are guessed or defined.
2. The nodes representing T-junctions are solved and their information (local pressure drop coefficients $A_{1,i}$, $A_{2,i}$, B_i and C_i) is transferred to the corresponding branch element.
3. The elements of each branch are solved sequentially in the flow direction. Each element is calculated from the outlet condition of the previous element, hence, the first branch element is calculated from the branch upstream manifold system node conditions. On one hand, the pressure drop coefficients of each element are added and a momentum equation for each branch is obtained (Equation 21). On the other, the enthalpy at the end of each branch is obtained after solving the in-tube two-phase flow model.
4. The whole net is solved on the basis of each branch pressure characterisation (Equation 22) and new flow distribution and node pressures are obtained. The enthalpies at the manifold system nodes are calculated with the energy conservation equation.
5. The previous nodes and branches values are compared with the recent ones. If the convergence criteria are not met then the algorithm must restart with the latest conditions (step 2).
6. The solid elements (tubes) are calculated (Equation 12) with both the new internal fluid flow maps and the updated heat exchanger external conditions (if they exist).
7. The tubes temperature maps are compared with the previous maps and if the convergence criteria are not met then the algorithm must restart with the latest temperature map (step 2).

Table 1
Manifold system conditions of Wang and Yu (3) experimental test.

Geometrical parameters	
Configuration	reverse as in Fig. 1(a)
Manifolds orientation	horizontal
Tubes orientation	horizontal
Dividing manifold diameter	13 mm
Combining manifold diameter	13 mm
Parallel tubes diameter, D_t	6.5 mm
Number of parallel tubes, N	10
Length of parallel tubes, L_t	1.12 m
Tube pitch, E	30 mm
Operational parameters	
External condition	adiabatic
Fluid	water
Flow type	single-phase flow
Inlet volumetric flow rate[a]	6.4 l/min

[a] Information obtained from Jones and Lior [4].

3. Flow distribution model validation

In this section, the present flow distribution model is compared against experimental data and numerical results for single- and two-phase flow manifold systems reported in the technical literature. The junction models used in this work are of the T-type and for round cross-section configurations. Therefore, the cross-sectional areas of the manifolds and the parallel tubes of the selected experimental cases are circular and the global geometric configuration is similar to that presented in Fig. 1(a). In the cases simulated with the present model, the influence of the recirculation phenomena inside manifolds must be low, as well as the flow alterations transmitted between consecutive junctions, in order to appropriately represent the manifold system by means of junctions and tubes. This restriction is also applicable to all the empirical information found for T-junctions. For this reason, a relatively large distance between two adjacent junctions (E, tube pitch) is recommended.

3.1. Single-phase flow through an adiabatic horizontal manifold system

Wang and Yu (3) proposed a numerical model and reported experimental results for manifold systems with single-phase water

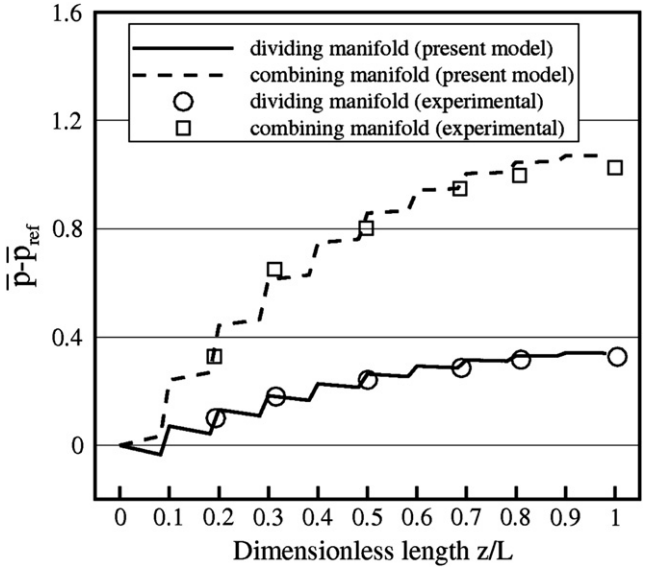

Fig. 4. Numerical predictions vs. Wang and Yu [3] experimental data.

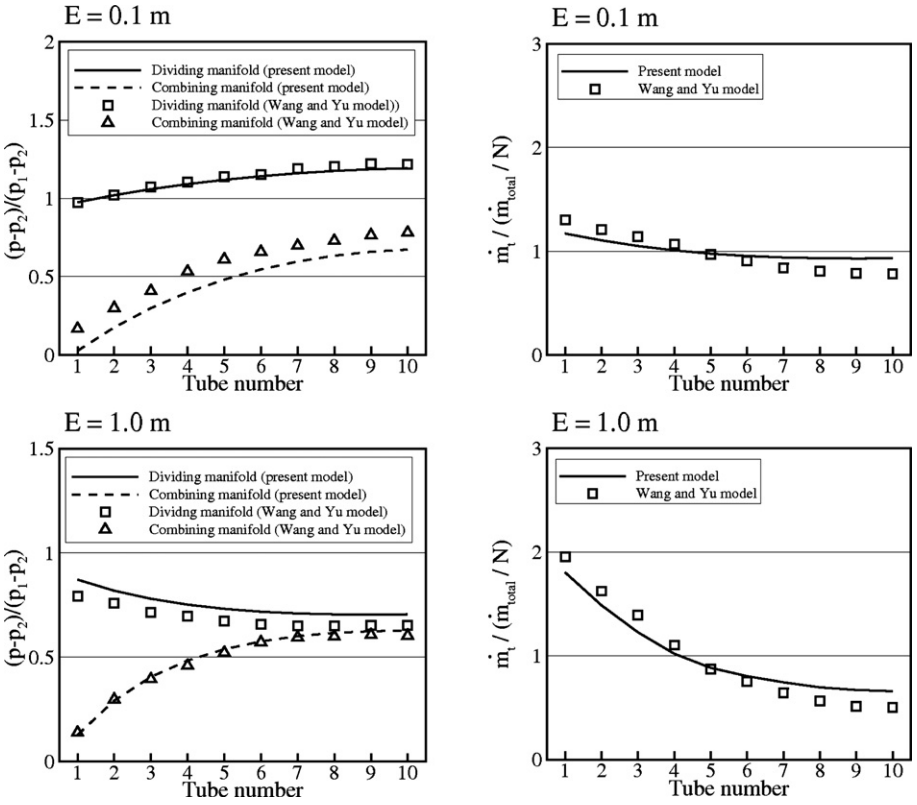

Fig. 5. Present numerical model vs. Wang and Yu [3] model (reverse configuration). The manifold system inlet and outlet pressures are denoted as p_1 and p_2 respectively.

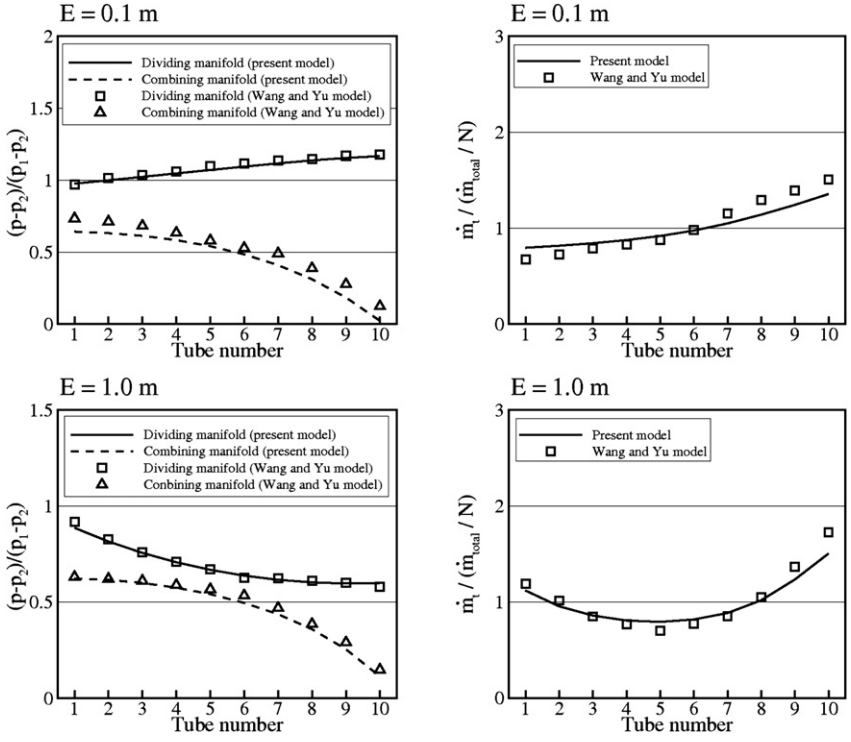

Fig. 6. Present numerical model vs. Wang and Yu [3] model (parallel configuration). The manifold system inlet and outlet pressures are denoted as p_1 and p_2 respectively.

Table 2
Manifold system conditions of Wang and Yu (3) numerical tests.

Geometrical parameters	
Configuration	reverse/parallel
Manifolds orientation	horizontal
Tubes orientation	horizontal
Dividing manifold diameter	25 mm
Parallel tubes diameter, D_t	12.5 mm
Number of parallel tubes, N	10
Length of parallel tubes, L_t	3 m
Tube pitch, E	0.1/1 m
Operational parameters	
External condition	adiabatic
Fluid	water
Flow type	single-phase flow
Inlet mass flow rate, $\dot{m}$	0.277 kg/s

Table 3
Manifold system conditions of Sivert (29) experimental tests (reference case conditions in bold).

Geometrical parameters	
Configuration	reverse as in Fig. 1(a)
Manifolds orientation	horizontal
Tubes orientation	vertical upward
Dividing manifold diameter	16 mm
Parallel tubes inner diameter, D_t	4 mm
Parallel tubes annular diameter	8 mm
Number of parallel tubes, N	10
Length of parallel tubes, L_t	0.9 m
Tube pitch, E	21 mm
Operational parameters	
External condition	non-adiabatic
Fluid	carbon dioxide
Flow type	two-phase flow
Inlet mass flow rate, $\dot{m}$	0.033 kg/s
Inlet gas weight fraction, x_g	0.14/**0.28**/0.43/0.54
Inlet saturation temperature	18.7 °C
Inlet counter-flow water temperature	30/**40**/50 °C

flow. Their work was focussed on studying the flow uniformity inside solar collectors and collector arrays. The experimental measurements were done in a manifold system made up of 10 parallel tubes placed between the dividing and the combining manifold as depicted in Fig. 1(a). The experimental test geometry and operational conditions are detailed in Table 1.

In Fig. 4, the experimental measurements of Wang and Yu [3] are compared against the numerical predictions of the present model. The dimensionless reference pressure ($\overline{p}_{ref}$) of the dividing manifold is calculated from its inlet pressure while for the combining manifold this value is calculated from its outlet pressure. In Fig. 4, the manifold length is denoted as L, and z is the manifold position where the fluid dimensionless pressure $\overline{p}$ is measured and calculated. The correlations needed to simulate the T-junctions and the fluid flow are reported in Sections 2.2 and 2.4, respectively.

The agreement shown in Fig. 4 is notably good (the differences between all the experimental data and their corresponding prediction were lower than 8%), considering that standard junction information has been used for the simulation. The numerical results allow to analyse the pressure evolution in both manifolds. It is interesting to observe how the main flow gains pressure through the dividing manifold. This phenomenon occurs because the pressure gains due to the sudden expansions of the main flow – when

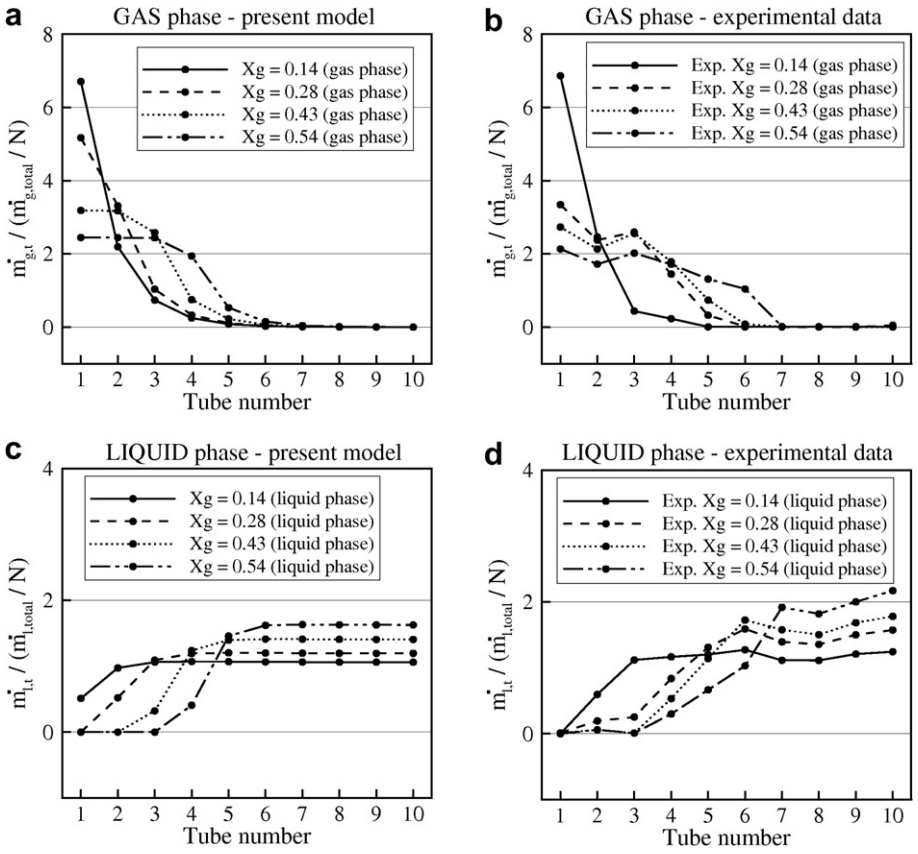

Fig. 7. Phase distribution for different manifold inlet gas weight fractions: (a,c) model predictions and (b,d) experimental data from Sivert [29].

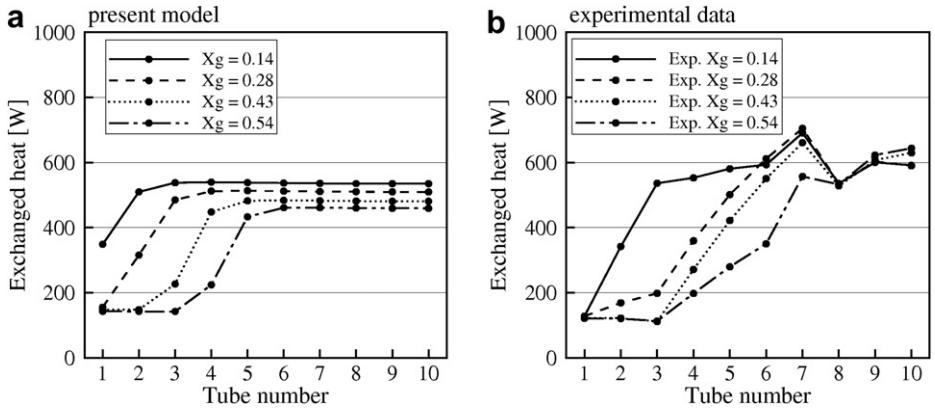

Fig. 8. Heat exchanged for different manifold inlet gas weight fractions: (a) model predictions and (b) experimental data from Sivert [29].

part of it is deviated through a parallel tube – are higher than the pressure losses due to friction along the manifold itself. Wang and Yu [3] stated that this behaviour is characteristic of the pressure regain type manifold systems. However, on the combining manifold, according to the main flow direction, the T-junction effect observed is opposite. In this case the pressure losses due to friction along the manifold are added to the pressure losses due to the main flow contractions – when incoming flows from the parallel tubes are added to the main flow.

An additional comparison was carried out between the present model and the numerical model of Wang and Yu [3] (Figs. 5 and 6). In this case, the comparison is focussed on a parametric study of the tube pitch (E) for two different manifold systems configurations: reverse, as in Fig. 1(a), and parallel (where the outlet of the combining manifold is in its opposite end). The conditions of the Wang and Yu numerical simulations are summarized in Table 2.

Their numerical study shows different trends of the pressure evolution through the distribution manifold: the pressure increases for small intervals between tubes (the pressure gain due to the junction effect is higher than the pressure loss due to the friction along the manifold), while it decreases for larger intervals (the friction pressure loss along the manifold becomes higher than the pressure gain due to the junction effect). In both manifold system configurations, the distance between parallel tubes has a little influence in the pressure profile of the combining manifolds. Thus, as it is shown in both Figures, the mass flow distribution is significantly related to the distribution manifold pressure profile. According to the simulations, the most uniform mass flow distribution is obtained with the reverse configuration and the smaller pitch ($E = 0.1$ m). A good agreement between the trends predicted with the present model and the model of Wang and Yu [3] is observed.

3.2. Two-phase flow through a non-adiabatic upwardly oriented manifold system

The experimental measurements of the manifold considered in this study were taken from Sivert [29] where typical car air-conditioning operating conditions and geometries were used. Sivert [29] presented a large number of experimental tests considering different refrigerants and a wide range of operational conditions.

The manifold was designed to simulate a car air-conditioning evaporator of approximately 5 kW capacity. The manifold was placed horizontally while the tubes were vertically upward oriented. The refrigerant used was carbon dioxide. In the experimental facility each parallel tube was heated by means of hot water flowing in counter-flow direction through a concentric annular tube. The validation study carried out in this section is based on the reference case and the experimental conditions detailed in Table 3. The flow distribution predictions of the present model are compared against Sivert (29) experimental data in Figs. 7–10.

In the numerical model, the manifolds are simulated as tubes with an insulation layer while the parallel tubes are simulated as double-pipe counter-flow heat exchangers. In the latter case, the

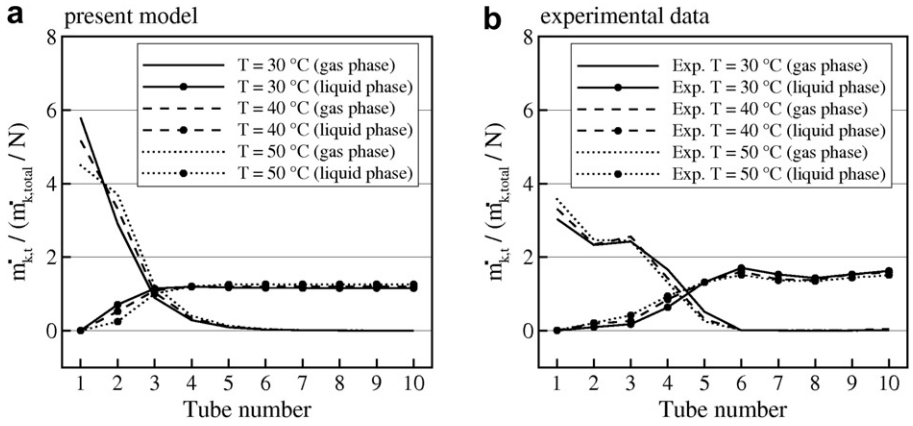

Fig. 9. Phase distribution for different counter-flow water inlet temperatures ($x_g = 0.28$): (a) model predictions and (b) experimental data from Sivert [29].

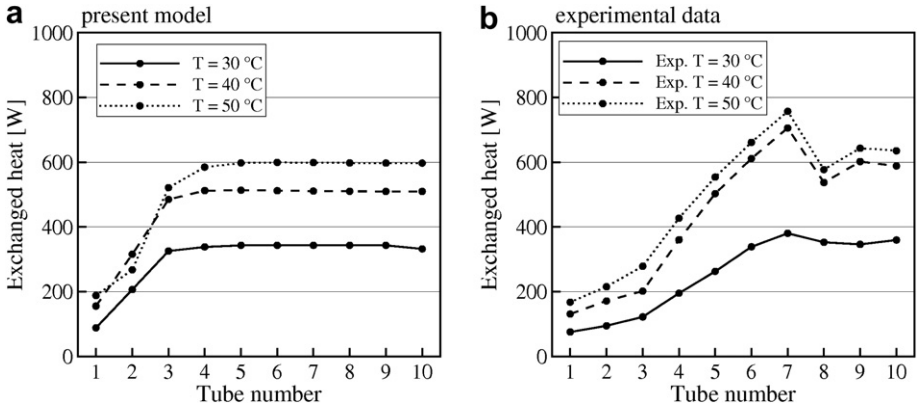

Fig. 10. Heat exchanged for different counter-flow water inlet temperatures ($x_g = 0.28$): (a) model predictions and (b) experimental data from Sivert [29].

secondary fluid and the external tube are simulated based on the same numerical model presented in Section 2.3. The correlations needed to simulate the T-junctions and the fluid flow are reported in Sections 2.2 and 2.4, respectively. The flow regime along the distribution manifold is predicted with the flow pattern map of Thome [17]. According to the map, the flow pattern predicted at the dividing manifold for all the simulated cases is of the stratified/stratified-wavy type.

Fig. 7 shows the inlet liquid and gas mass flow ratios of the manifold system parallel tubes at different distribution manifold inlet gas weight fractions. The evolution of the gas and liquid mass flow ratios profile is very similar between the numerical predictions (Fig. 7a and c) and the experimental measurements (Fig. 7b and d). Due to the higher moment of inertia of the liquid phase and the vertical upward orientation of the tubes, the gas and the liquid phases are preferably deviated through the first and the last tubes, respectively. It can be noticed that for each test there is a tube in the manifold system from which the liquid mass flow ratio is greater than the gas flow ratio in all the subsequent tubes. This tube position moves towards the manifold end as the manifold inlet gas weight fraction increases. This behaviour is observed in the model predictions as well as the experimental data.

In Fig. 8 the heat exchanged by each tube at different distribution manifold inlet gas weight fractions is depicted. In this case, although the mean prediction error $\left(\sum_{i=1}^{n}\left(\frac{|Q_{exp}-Q_{calc}|}{Q_{exp}}\right)_i/n\right)$ of all the experimental points is significant (30%), the general trends of the experimental data are reasonably well predicted. The liquid mass flow ratio profile is closely related to the profile of the heat exchanged in tubes due to the heat transfer characteristics of the liquid phase (much higher heat transfer coefficient than the gas phase). Poor heat transfer is observed in tubes with low liquid mass flow ratio. In fact, the liquid phase observed in tubes 1 to 4 is negligible for the case of $x_g = 0.54$ where mostly of the heat exchanged by the whole system is done by tubes 6 to 10. The less accurate prediction occurs for the case of $x_g = 0.28$ because its phase distribution was also less accurately predicted.

Fig. 9 shows the influence of the double-pipe secondary fluid inlet temperature in phase distribution. In the model predictions as well as the experimental data, the mass flow ratio profiles are not affected when the heat load applied to the tubes changes.

Fig. 10 shows the profile of the heat exchanged by tubes for different heat loads. The mean prediction error is significant (32%) but the general trends of the experimental data of Sivert [29] are well predicted. The predicted heat profile slope between tubes number 1 and 4 is rather steep compared to the experimental cases where the corresponding slope goes from tube number 3 to 6. This discrepancy is closely related to the differences between the numerical and the experimental liquid mass flow ratio profiles of Fig. 9.

The mean prediction error of the simulated cases is significant due to the high level of empiricism used by the model and the limiting conditions of the correlations. However, a qualitative agreement between the obtained numerical predictions and the experimental data is observed. The general trends of the simulated cases (mass flow distribution, exchanged heat profile, etc.) are well predicted by both the T-junction models and the fluid flow model. Thus, both models were successfully coupled in the global flow distribution algorithm.

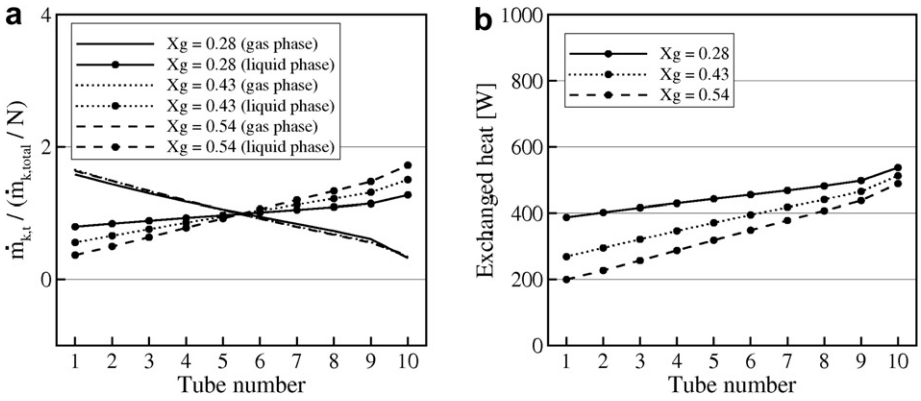

Fig. 11. Model predictions for horizontal manifold with horizontal oriented tubes at different inlet gas weight fractions: (a) phase distribution and (b) heat exchanged by tubes.

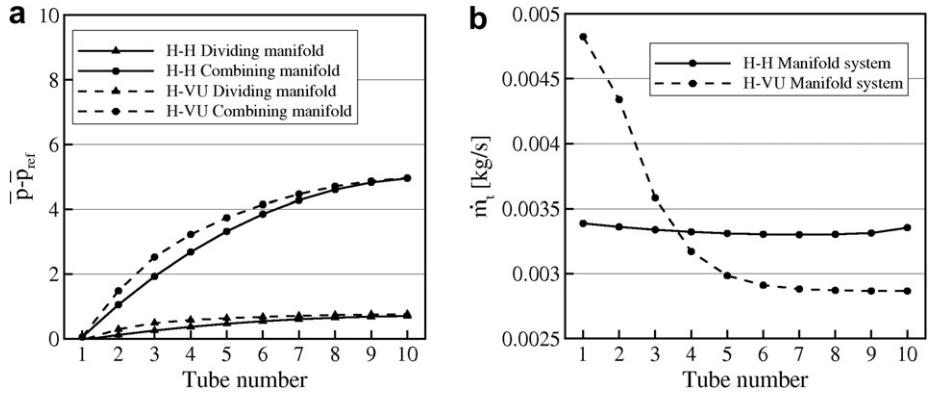

Fig. 12. Manifold system at two orientations (H–H and H–VU): (a) manifold pressure profiles and (b) parallel tube mass flows.

4. Numerical results

In this section, a numerical comparative study is carried out in order to show the model capabilities. The two-phase flow manifold system with upwardly oriented parallel tubes (H–VU) that was validated in the Section 3.2 is simulated for a different orientation: horizontal manifold with horizontal parallel tubes (H–H). In this case, the phase separation in dividing T-junctions is simulated with the model of Tae and Cho [12] which consists on an extended version of the Hwang et al. model [10]. This model can be used in horizontal junctions with diameter reduction and may require specific geometric relations depending on the flow regime. According to the flow pattern map of Thome [17] the flow regime through the dividing manifold of the simulated cases was of the type stratified/stratified-way. Therefore, the corresponding geometric relations have been derived for this study. The results are presented in Figs. 11–13 where a numerical comparison between both configurations is carried out as no experimental data were available for the horizontal configuration. The flow conditions are the same of the reference case studied in Section 3.2.

Fig. 11(a) shows the inlet liquid and gas mass flow ratios of the H–H manifold system parallel tubes at different dividing manifold inlet gas weight fractions. This parameter has little influence in the phase distribution in contrast to the H–VU manifold (see Fig. 7a and c). For all the simulated gas weight fractions, the gas mass flow ratio is greater than the liquid mass flow ratio in the first five tubes and the opposite situation is seen in the last five tubes. The liquid mass flow ratio increases linearly from tube number 1 to 10 while the gas mass flow ratio decreases linearly. In fact, the slope of the liquid mass flow ratio profile gently increases as the manifold inlet gas weight fraction increases but the gas mass flow ratio profile slope remains almost equal. This situation is completely different for the H–VU manifold where the gas and liquid mass flow ratio profiles present steeper variations (Fig. 7). Fig. 11(b) shows the heat exchanged by each tube in the H–H manifold system. The heat exchanged increases progressively from tube 1 to 10 due to the increasing linear tendency of the liquid mass flow ratio profile.

Fig. 12 presents the manifold pressure profiles and the mass flow rate distribution of the reference manifold system ($x_g = 0.28$). Fig. 12(a) shows that the dividing and combining manifold pressure profiles for both the H–H and the H–VU manifold system are similar, however, Fig. 12(b) shows a very unequal mass flow distribution between both configurations. The H–H manifold presents a more uniform distribution because the liquid and gas phases are more evenly distributed.

The differences between both orientations may be also seen in Fig. 13 where the fluid temperature and the inner tube temperature evolution along tubes are plotted for the reference case ($x_g = 0.28$). In fact, only two representative tubes are studied: one from the first part of the manifold (tube number 2), and the other from the last part of the manifold (tube number 9). In Fig. 13(a) it can be observed that the thermal behaviour of tube number 9 is similar for both configurations (single-phase starts at 0.6 m). This is not the case for tube number 2, where the single-phase flow condition starts at 0.3 m and 0.45 m for the H–VU and H–H manifold systems respectively. Consequently, in both cases more heat is transferred by tube number 9 due to its longer lasting two-phase flow condition. However, the fluid temperature profile difference between tube number 2 and 9 is greater for the H–VU manifold system due to the more significant gas phase predominance in its first tubes.

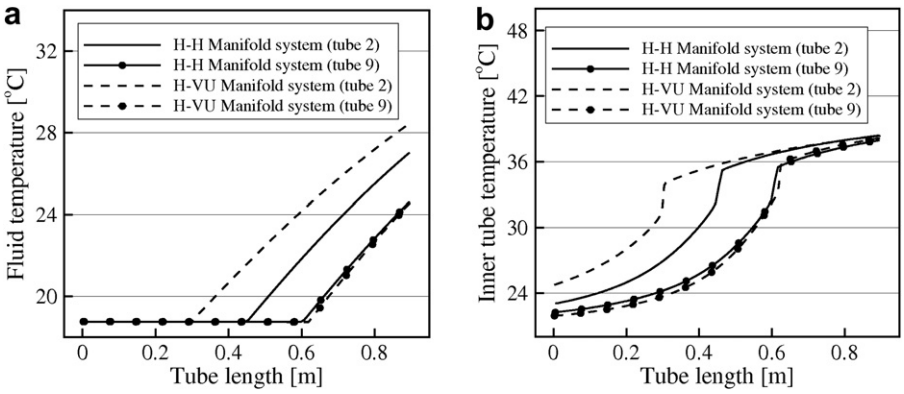

Fig. 13. Representative tubes of both manifold systems (H–H and H–VU): (a) fluid temperature evolution and (b) inner tube temperature evolution.

This is directly related to the tube temperature evolution as seen in Fig. 13(b).

In both configurations, H–H and H–VU, the heat transferred by the last tubes is greater compared to the first tubes. However, the corresponding heat transfer profiles are very different as shown in Figs. 10(b) and 11(b). This is mainly due to the flow distribution which is more uniform in the H–H manifold system.

5. Concluding remarks

A numerical model for predicting the flow distribution in multiple parallel tubes has been detailed and compared against experimental data together with other numerical models found in the open literature. The simulations have been carried out for different manifold systems, considering a wide variety of aspects: i) single-phase and two-phase flows; ii) reverse and parallel manifold system arrangement; iii) horizontal manifolds with both horizontal and upward oriented parallel tubes; iv) different operating conditions (inlet mass flow rate, inlet gas weight fraction etc.); v) different geometric sizes; and vi) different heat loads on parallel tubes. The model shows good qualitative agreement against experimental data as the effects of the studied parameters are well predicted. The model accuracy depends on the availability and appropriate selection of T-junction models as well as the manifold geometry which must be adequate to be represented by means of tubes and junctions. The numerical results presented in the last section allow to show the capabilities and level of detail of the developed model.

Acknowledgement

This work has been financially supported by the Ministerio de Eduación y Ciencia, Secretaría de Estado de Universidades e Investigación, Spain (ref. ENE2006-11099/CON).

Nomenclature

Bo	boiling number, $\frac{\dot{q}}{G\Delta h}$
D	tube diameter, m
E	tube pitch, mm
e	specific energy, J kg^{-1}
Fr	Froude number, $\left(Fr = \frac{G^2}{gD\rho_h^2}\right)$
f	friction factor
G	mass velocity, kg m^{-2} s^{-1}
g	acceleration due to gravity, m s^{-2}
h	enthalpy, J kg^{-1}
L	length, m
$\dot{m}$	mass flow rate, kg s^{-1}
$\dot{m}_{total}$	manifold system mass flow rate, kg s^{-1}
N	number of parallel tubes
Nu	Nusselt number, $\left(Nu = \frac{\alpha D}{\lambda}\right)$
n	number of measurements
p	pressure, *Pa*
$\overline{p}$	dimensionless pressure, $\left(\overline{p} = \frac{p}{\rho v_{in}^2}\right)$
Q	heat, W
$\dot{q}$	heat flux, W m^{-2}
R	radius, m
Re	Reynolds number, $\left(Re = \frac{GD}{\mu}\right)$
S	cross-sectional area, m^2
T	temperature, K
v	velocity, m s^{-1}
v_{sl}	liquid superficial velocity, m s^{-1}
We	Weber number, $\left(We = \frac{G^2 D}{\rho_h \sigma}\right)$
x_g	gas weight fraction
z	axial position, m

Greek symbols

α	heat transfer coefficient, W m^{-2} K^{-1}
Δh	latent heat, J kg^{-1}
Δp	pressure variation, *Pa*, $(\Delta p_{i-j} = p_i - p_j)$
Δz	axial step, m
ϵ_g	void fraction
ε	absolute roughness, m
θ	tube inclination angle, *rad*
λ	thermal conductivity, W m^{-1} K^{-1}
μ	dynamic viscosity, kg m^{-1} s^{-1}
ξ	resistance coefficient, accuracy
ρ	density, kg m^{-3}
ρ_h	homogeneous density, kg m^{-3}, $\left(\rho_h = \frac{\rho_l \rho_g}{x_g \rho_l + (1-x_g)\rho_g}\right)$
σ	surface tension, N m^{-1}
τ	shear stress, *Pa*
ϕ	discretized variable, two-phase flow multiplier

Subscripts

br	branch
c	kinetic
cb	convective boiling
d	destination
ext	external
g	gas
i	grid position
in	inlet
k	phase (gas or liquid)
l	liquid
nb	nucleate boiling
o	origin
p	potential
ru	run
t	parallel tube
tp	two-phase

References

[1] M. Watanabe, M. Katsuta, K. Nagata, General characteristics of two-phase flow distribution in a multipass tube, heat transfer. Japanese Research 24 (1) (1995) 32–44.
[2] R.A. Bajura, E.H. Jones Jr., Flow distribution manifolds. Journal of Fluids Engineering 98 (1976) 654–665.
[3] X.A. Wang, P. Yu, Isothermal flow distribution in header systems. International Journal of Solar Energy 7 (1989) 159–169.
[4] G.F. Jones, N. Lior, Flow distribution in manifolded solar collectors with negligible buoyancy effects. Solar Energy 52 (3) (1972) 289–300.
[5] A.C. Mueller, J.P. Chiou, Review of various types of flow maldistribution in heat exchangers. Heat Transfer Engineering 9 (2) (1988) 36–50.
[6] Y. Hwang, D.H. Jin, R. Radermacher, Refrigeration distribution in minichannel evaporator manifold. HVAC and Research 13 (4) (2007) 543–555.
[7] A. Marchitto, F. Devia, M. Fossa, G. Guglielmini, C. Schenone, Experiments on two-phase flow distribution inside parallel channels of compact heat exchangers. International Journal of Multiphase Flow 34 (2008) 128–144.
[8] O. García-Valladares, C.D. Pérez-Segarra, J. Rigola, Numerical simulation of double-pipe condensers and evaporators. International Journal of Refrigeration 27 (6) (2004) 656–670.
[9] W. Seeger, J. Reimann, U. Muller, Two-phase flow in a T-junction with a horizontal inlet, part I: phase separation. International Journal of Multiphase Flow 12 (4) (1986) 575–585.
[10] S.T. Hwang, H.M. Soliman, R.T. Lahey Jr., Phase separation in dividing two-phase flows. International Journal of Multiphase Flow 14 (4) (1988) 439–458.
[11] F. Marti, O. Shoham, A unified model for stratified-wavy two-phase flow splitting at a reduced T-junction with an inclined branch arm. International Journal of Multiphase Flow 23 (4) (1997) 725–748.
[12] S. Tae, K. Cho, Two-phase split of refrigerants at T-junction. International Journal of Refrigeration 29 (7) (2006) 1128–1137.
[13] I.E. Idelchik, Handbook of Hydraulic Resistance. CRC Press, 1994.

[14] C. Oliet, N. Ablanque, J. Rigola, C.D. Pérez-Segarra, A. Oliva, Numerical studies of two-phase flow distribution in evaporators, in: Proceedings of the 22th International Congress of Refrigeration, 2007.
[15] J.R. Buell, H.M. Soliman, G.E. Sims, Two-phase pressure drop and phase distribution at a horizontal tee junction. International Journal of Multiphase Flow 20 (5) (1994) 819–836.
[16] H. Schmidt, R. Loth, Predictive methods for two-phase flow pressure loss in tee junctions with combining conduits. International Journal of Multiphase Flow 20 (4) (1994) 703–720.
[17] J.R. Thome, Update on advances in flow pattern based two-phase heat transfer models. Experimental Thermal and Fluid Science 29 (3) (2005) 341–349.
[18] S.W. Churchill, Frictional equation spans all fluid flow regimes. Chemical Engineering 84 (24) (1977) 91–92.
[19] L. Friedel, Improved friction pressure drop correlation for horizontal and vertical two-phase pipe flow. European Two-Phase Flow Group Meeting, Ispra, Italy. Paper E2 (1979).
[20] V. Gnielinski, New equations for heat and mass transfer in turbulent pipe and channel flow. International Chemical Engineering 16 (2) (1976) 359–368.
[21] K.E. Gungor, R.H.S. Winterton, A general correlation for flow boiling in tubes and annuli. International Journal of Heat and Mass Transfer 29 (3) (1986) 351–358.
[22] M.G. Cooper, Saturation nucleate pool boiling – a simple correlation. Institution of Chemical Engineers Symposium Series 86 (1984) 785–793.
[23] F.W. Dittus, L.M.K. Boelter, Heat Transfer in Automobile Radiators of the Tubular Type, vol. 2, University of California Publications on Engineering, 1930, pp. 433.
[24] K.E. Gungor, R.H.S. Winterton, Simplified general correlation for saturated flow boiling and comparisons of correlations with data. Chemical Engineering Research and Design 65 (2) (1987) 148–156.
[25] D.C. Groeneveld, Post-dryout heat transfer at reactor operating conditions, ANS conference No. 730304 (1973) 321–350.
[26] A. Premoli, D. Francesco, A. Prima, An empirical correlation for evaluating two-phase mixture density under adiabatic conditions. European Two-Phase Flow Group Meeting, Milan, Italy (1970).
[27] S.V. Patankar, Numerical Heat Transfer and Fluid Flow. McGraw-Hill, New York, 1980.
[28] C. Oliet, Numerical simulation and experimental validation of fin-and-tube heat exchangers, Ph.D. thesis, Universitat Politècnica de Catalunya (2006).
[29] V. Sivert, Two-phase flow distribution in heat exchanger manifolds, Ph.D. thesis, Norwegian University of Science and Technology (2003).